Assessment of a constraint-based routing algorithm for translucent 10 Gbits/s DWDM networks considering fiber nonlinearities

Stephan Pachnicke,* Tom Paschenda, and Peter Krummrich

High Frequency Institute, Dortmund University of Technology, Friedrich-Wöhler-Weg 4, 44221 Dortmund, Germany
**Corresponding author: stephan.pachnicke@udo.edu*

Received December 11, 2007; revised February 18, 2008; accepted February 22, 2008; published March 31, 2008 (Doc. ID 90726)

We present a constraint-based routing (CBR) approach for real-time operation considering both linear as well as nonlinear signal quality degrading effects in a heterogeneous network infrastructure. Different novel routing algorithms are assessed regarding their blocking probabilities. Furthermore, regenerator pools are placed at a limited number of nodes selected by a heuristic algorithm taking into account the physical impairments. It is shown that CBR together with intelligent regenerator placement can decrease the blocking probability significantly. © 2008 Optical Society of America

OCIS codes: 060.0060, 060.4251.

1. Introduction

For operating a dynamic optical network of pan-European or trans-American dimensions, it is essential to consider physical transmission impairments in the routing process because of potentially very long transparent path lengths. Constraint-based routing (CBR) has been a subject of intensive research in the last several years (e.g., [1–4]). In this paper we present a novel CBR approach based on analytical models for the dominant linear and nonlinear signal quality degrading effects in 10 Gbits/s nonreturn-to-zero (NRZ) on–off keying (OOK) systems. Currently, most installed services are 10 Gbits/s, and future automatically switched optical networks (ASONs) are likely to provide dynamic configuration of 10 Gbits/s λ channels. As a topology for our study, we have chosen the COST266 network (large topology), which is a pan-European reference network with a total of 37 nodes and 57 links [5]. For this network, demands have been defined based on a population-based model [6]. As a figure of merit (FOM) we evaluate the wavelength blocking probability. To facilitate transmission over very long path lengths, pools with a fixed number of regenerators have been placed at certain nodes determined by a heuristic algorithm. The regenerator sites are selected based on a model taking into account the physical degradation effects. Due to the high cost of optical–electrical–optical (OEO) conversion, as few regenerators as possible should be deployed. In contrast to fully transparent transmission, a network with selective regeneration at certain sites is called a translucent network.

Combining intelligent regenerator placement and CBR yields a significantly reduced blocking probability. Our novel online CBR approach takes into account the current traffic situation on the links. Furthermore, it offers the flexibility to assess a heterogeneous network infrastructure with different fiber types and a varying dispersion map. The exact assessment of the signal quality based on the current traffic situation using fast analytical methods permits up to five times more traffic in a network compared to routing with worst-case estimations (for a blocking probability of 3%).

The paper is organized as follows. In Section 2 the investigated reference network is presented. Furthermore, the heuristic is explained, which has been used to assign physical parameters such as fiber lengths and dispersion compensation maps to the links defined in the reference network. Section 3 deals with the CBR algorithms examined in this paper. Our CBR algorithms consider the dominant linear as well as nonlinear impairments for 10 Gbits/s NRZ-OOK transmission systems. We include

amplified spontaneous emission (ASE) noise, filter cross talk, cross-phase modulation (XPM), and four-wave mixing (FWM). The heuristic for the placement of the regenerators is explained in Section 4. In Section 5 we compare the blocking probability for different routing algorithms and scenarios. We conclude our results in Section 6.

2. Investigated Scenario

In this paper we investigate the COST266 reference network (large topology) [5] as an example for a large-scale network. COST266 has pan-European dimensions (37 nodes and 57 links) in a mesh topology (Fig. 1). Simulations with our analytical models (see Section 3 for more details) have shown that there are long paths with good signal quality (maximum reach for $Q > 15.56$ dB is 2220 km) and short paths with poor quality (minimum reach is 1280 km), as depicted in Fig. 2, making an accurate assessment of the signal quality at the end of the path for a requested demand highly desirable. Each point shown in Fig. 2 represents a path between any combinations of two nodes. Because the three shortest-disjoint paths have been investigated, there exist paths of up to approximately 6000 km total length. The Q factor is calculated as defined in Eq. (13) incorporating ASE noise as an optical signal-to-noise ratio (OSNR) penalty and the nonlinear effects as well as filter cross talk as additional Q penalties.

Furthermore, simulations have shown that the nonlinear fiber effects of XPM and FWM cannot be neglected for very long paths in the COST266 network if a 10 Gbits/s NRZ-OOK modulation format is used. This is why in our CBR approach XPM and FWM have been included by analytical models presented in [7]. In the COST266 reference network only link lengths and demands have been defined. For the assessment of the signal quality, however, it is essential to know the physical parameters of the network elements and individual fiber spans. For this purpose a heuristic approach has been developed based on realistic assumptions motivated by deployed networks. The span lengths have been calculated once from a random process with a Gaussian distribution with a mean value of $\mu = 80$ km (a common value for the distance between two amplifier huts in today's deployed networks) and a standard deviation of $\sigma = 5$ km. For the dispersion compensation fiber (DCF) modules a granularity of 10 km standard single-mode fiber (SSMF) equivalent (i.e., −170 ps/nm) has been assumed for both transmission fiber types. The DCF modules have been chosen in such a way that some residual dispersion is left in each span (distributed undercompensation scheme) resulting in less severe accumulation of the nonlinear fiber effects. By this scheme an average undercompensation of 85 ps/nm/span is achieved along the links. At the nodes the residual dispersion is minimized because some channels may be dropped and others may be added.

We assumed the entire network to consist of either SSMF with a dispersion parameter of $D = 17$ ps/nm/km or nonzero dispersion-shifted fiber (NZDSF) with $D = 4$ ps/nm/km. Furthermore, the following parameters have been used: launch power

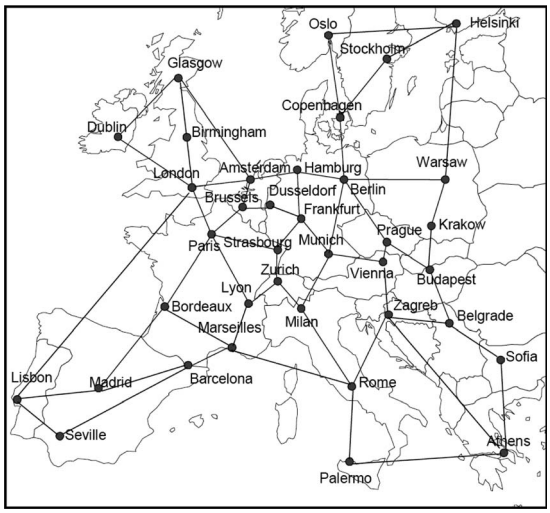

Fig. 1. COST266 reference network (large topology) [5].

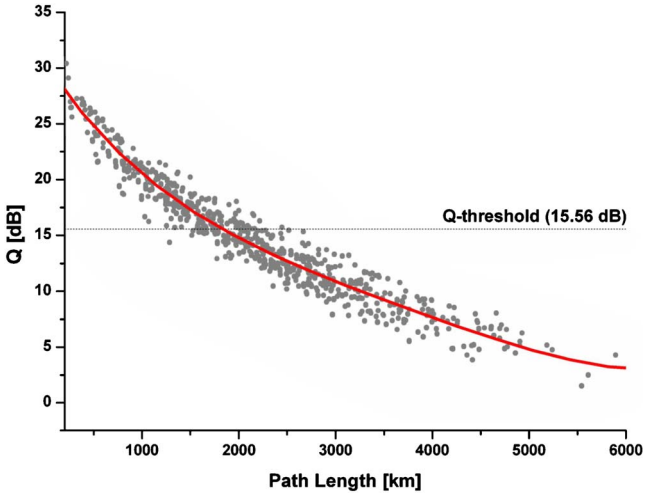

Fig. 2. Maximal reach in the investigated network. Each point represents a path in the COST266 network. Results are shown for the network based on SSMF and obtained from our analytical model. No OEO regeneration.

$P_{\text{launch}}=3$ dBm/ch, launch power $P_{\text{launch,DCF}}=-3$ dBm/ch, attenuation constant $\alpha=0.23$ dB/km, nonlinearity constant $\gamma_{\text{SSMF}}=1.37$ (W km)$^{-1}$, and nonlinearity constant $\gamma_{\text{NZDSF}}=2$ (W km)$^{-1}$.

We assume a channel plan with a maximum of 80 wavelengths per link spaced at 50 GHz. For the erbium-doped fiber amplifers (EDFAs) a noise figure of $F_o=5.5$ dB has been selected. It is important to mention that such a network scenario requires very flexible physical models because the system parameters vary from span to span. Furthermore, it is not possible to calculate the transmission performance for a single span and easily scale it to the total distance because the dispersion management is varying.

3. CBR Algorithms

The analytical models that we used for the assessment of the signal quality are outlined in the following. The accuracy of our models has already been discussed in [7]. In recirculating loop experiments for a transmission system with 20 spans, excellent agreement with the analytical XPM model has been shown. In further experiments, FWM impairments have been investigated, and very good agreement with the analytical FWM model has been obtained for different dispersion compensation maps and a transmission distance up to 25 spans.

In this section we show how the results for the different physical degradation effects can be aggregated to a single figure of merit (Q factor). Finally, the different CBR algorithms used in this work are described.

3.A. ASE Noise

EDFAs always degrade the OSNR. This comes from the fact that spontaneous emission inevitably occurs along with stimulated emission. For a single EDFA with gain G the OSNR is defined as follows:

$$\text{OSNR}=\frac{GP_{\text{in}}}{P_{\text{ASE}}}=\frac{P_{\text{in}}}{F_o h f \Delta f_{\text{opt,ref}}}. \tag{1}$$

In Eq. (1) P_{in} stands for the (channel) launch power, h is Planck's constant, f is the optical center frequency (here $f=193.1$ THz), and $\Delta f_{\text{opt,ref}}$ is the optical reference bandwidth (here $\Delta f_{\text{opt,ref}}=12.5$ GHz, equivalent to $\Delta\lambda=0.1$ nm at $\lambda=1550$ nm). To describe the degradation of the OSNR, a noise figure F_o is used (here $F_o=5.5$ dB), which is defined as the ratio of the OSNR before and after the amplifier for a shot-noise-limited signal. For a concatenation of EDFAs along the optical path the OSNR is calculated from the well-known formula for the accumulation of noise in a cascade of amplifiers (e.g., [8]).

3.B. XPM

XPM causes a modulation of the optical phase of a given channel through the variation of the effective refractive index due to other intensity-modulated channels propagating in the same fiber. The modulation of the optical phase is converted into intensity modulation of the signal by dispersion, leading to an amplitude-noise-like distortion. We used an analytical model first suggested by [9], where XPM degradations are assessed by a transfer function in the frequency domain derived from a pump-probe model. The main features of the analytical model are described below. More details can be found in [10].

In the following, the index i stands for the probe channel number and the index k for the pump channel number. The number of fiber spans is denoted by N. The transfer function can be calculated by

$$H_{\mathrm{XPM},ik}(\omega) = 2g_{\mathrm{net}} \sum_{l=1}^{N} \gamma(l) \exp(j\omega D_I^{(l-1)} \Delta\lambda_{ik}) \prod_{n=1}^{l-1} (\exp(-\alpha_l L_l) g_k) \times \left(\frac{1}{(a_{ik})^2 + (2b_i)^2} [a_{ik}(C_i - 2D_i(l)) - 2b_i] + \frac{\sin(C_i)}{a_{ik}} \right), \tag{2}$$

with the net power gain g_{net} from the transmitter to the receiver, the nonlinearity coefficient $\gamma^{(l)}$ of the lth fiber, the accumulated inline dispersion $D_I^{(l-1)}$ in front of the lth segment, the channel spacing $\Delta\lambda_{ik}$ between channels i and k, the length L_l of the lth transmission fiber, the attenuation constant α_l of the fiber, the gain g_k of the booster in front of the lth transmission fiber, and

$$C_i = \frac{\omega^2 \lambda_i^2}{4\pi c} D_R, \tag{3}$$

$$D_i^{(l)} = \frac{\omega^2 \lambda_i^2}{4\pi c} D_I^{(l-1)}, \tag{4}$$

$$a_{ik} = \alpha - j\omega D \Delta\lambda_{ik}, \tag{5}$$

$$b_i = \omega^2 D \lambda_i^2 / (4\pi c_0), \tag{6}$$

where λ_i denotes the wavelength of the ith channel, c_0 is the speed of light, D_R is the residual dispersion at the end of the system, and D is the dispersion coefficient of the lth fiber. Equation (2) has the great advantage that it allows one to model systems with arbitrary dispersion compensation—varying on a span-by-span basis—and supports different fiber types in each span. The nonlinearity of the DCF has been neglected in this approach. Equation (2) has to be evaluated for each pump channel $k = 1, \ldots, M$. To obtain an analytical expression for the XPM-induced noiselike variance of the photocurrent the following approach is used:

$$\sigma_{\mathrm{XPM},i}^2 = \bar{P}(0)^2 \sum_{j=1, j\neq i}^{M} \frac{1}{2\pi} \int_{-\infty}^{+\infty} |H_{XPM,ij}(\omega)|^2 |H_{\mathrm{opt\ filter}}(\omega)|^2 \mathrm{PSD}_j(\omega) \mathrm{d}\omega, \tag{7}$$

with the average (channel) launch power $\bar{P}(0)$ into the fiber, the XPM transfer function $H_{\mathrm{XPM},ij}$, the filter function of the optical filter $H_{\mathrm{opt\ filter}}$, the total number of channels M, and the power spectral density of the pump channel PSD_j [11],

$$\mathrm{PSD}_{\mathrm{NRZ}}(\omega) = \frac{P_{\mathrm{max}}^2}{4} \left[\left| \frac{\cos(RT\omega/2)}{1 - (RT\omega/\pi)^2} \frac{\sin(T\omega/2)}{T\omega/2} \right|^2 + \delta(\omega) \right], \tag{8}$$

where P_{max} is the peak power at the beginning of the fiber, R is the cosine roll-off factor, and T is the bit duration. In [7] the analytical results obtained with our model have been compared to pump-probe experiments in a recirculating loop showing excellent agreement.

3.C. FWM

FWM leads to the generation of a new wave through the third-order electric susceptibility of a fiber, when three waves interact. For a high efficiency of FWM both frequency ($f_{ijk}=f_i+f_j-f_k$) and phase conditions ($\Delta\beta\approx 0$) need to match. If the channels are equally spaced in frequency in a WDM system, the new waves generated by FWM will occur at channel frequencies and thus will contribute to cross talk. In case of full in-line dispersion compensation the FWM cross talk becomes maximum since the FWM products add constructively along the transmission line.

The analytical model used for the assessment of the FWM degradation in this paper is based on a single span continuous-wave approximation [12]. The amplitude of an FWM product at frequency m, which is generated by waves i, j, and k, can be calculated in the general case from the following equation [12]:

$$A_{m,ijk}(l_1,l_2)=j\gamma\left(\frac{d}{3}\right)A_i(0)A_j(0)A_k^*(0)\int_{z=l_1}^{l_2}\exp(-\alpha z-j\Delta\beta_{ijk}z)\mathrm{d}z, \tag{9}$$

where A is the amplitude of the envelope of the different waves, γ is the nonlinearity constant of the fiber, and α is the attenuation constant. l_1 and l_2 are the absolute positions on the fiber, measured from the beginning of the transmission system. The degeneracy factor d has a value of 3 for $i=j$ (two-tone product) and a value of 6 for $i\neq j$ (three-tone product). In Eq. (9) the amplitude distortion due to dispersion has been neglected. This is valid for low (local) dispersion fibers and moderate bit rates (i.e., 10 Gbits/s systems) where FWM degradation is dominant. The phase matching between the different waves can be calculated from [12]

$$\Delta\beta=\beta_i+\beta_j-\beta_k-\beta_{ijk}=\frac{2\pi\lambda^2}{c_0}(f_i-f_k)(f_j-f_k)\left[D-\frac{\lambda^2}{c_0}\left(\frac{f_i+f_j}{2}-f\right)S\right]. \tag{10}$$

To take into account the random nature of the modulated signal three-tone products are weighted by a factor of 1/8 and two-tone products by a factor of 1/4. This comes from the probability in a pseudorandom binary sequence (PRBS), which is 0.5 for a mark.

The power of a single FWM product at the end of a single section of fiber of length L can be calculated by

$$P_{m,ijk}(L)=\left(\frac{d}{3}\gamma\right)^2 e^{-\alpha L}P_i(0)P_j(0)P_k(0)\left|\frac{\exp(-\alpha L-j\Delta\beta_{ijk}L)-1}{-\alpha-j\Delta\beta_{ijk}}\right|^2. \tag{11}$$

An extension to multispan systems has been shown in [13]. From the sum of all FWM products falling in the regarded channel, a variance can be computed, which can be treated similar to ASE noise:

$$\sigma^2_{\mathrm{FWM}}=2P_{ch}\sum_{ijk}P_{m,ijk}. \tag{12}$$

In laboratory experiments with a recirculating loop, excellent agreement with the analytical model has been shown (as already published in [7]).

3.D. Filter Cross Talk

In our studies we assumed a node architecture as shown in Fig. 3. The node contains EDFAs at the inputs and outputs compensating for the switching losses. We assumed a total loss of 10 dB inside the node. In transparent optical cross-connects (OXC) two different forms of cross talk may occur: intraband and out-of-band cross talk. The former will occur if a channel is dropped with insufficient isolation and a certain amount of power remains at the wavelength. Consequently, cross talk will arise if a new channel is added at the same frequency. Out-of-band cross talk is caused by the neighboring channels due to imperfect filter edge steepness. Both forms of cross talk depend very much on the architecture of the OXCs [14]. OXCs must allow optical pass-through for express channels as well as add–drop for local traffic. Furthermore, certain wavelengths may be passed to a regenerator bank (Fig. 3). Because many different designs for OXCs have been suggested in the literature and are deployed in real networks, in this paper a Q penalty of 1 dB due to cross talk has been assumed

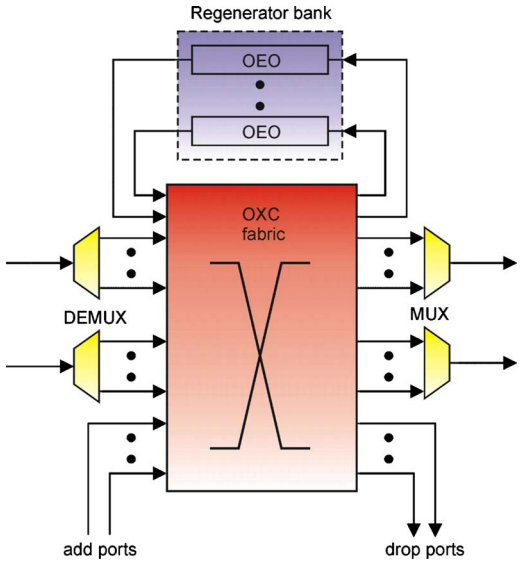

Fig. 3. Node architecture with optional OEO regeneration [17].

for each OXC included in the transmission path to keep the results more generic. The penalties are added if several OXCs are cascaded along the path leading to a worst-case approximation of the cross talk. In [14] Q penalties from filter concatenation with different cross talk levels have been investigated in great detail confirming our assumption of a 1 dB Q-factor penalty per passed OXC (compare Fig. 23 in [14]).

3.E. Accumulation to a Single FOM

In our studies we considered the dominant physical degradation effects only. Due to the dispersion management no significant degradation caused by residual group-velocity dispersion (GVD) can occur, and thus GVD is not considered here. Also polarization mode dispersion (PMD) has not been accounted for. We do not expect significant system penalties due to PMD for the investigated 10 Gbits/s NRZ-OOK transmission format because we assume that next-generation transparent optical networks will be built with newer—post-1995—fibers with low PMD coefficients (i.e., $0.05\ \text{ps}/\sqrt{\text{km}}$). If desired, PMD-induced penalties can be included by the approach shown in [10]. Furthermore, we do not consider system impairments due to the nonlinear fiber effects self-phase modulation (SPM) and stimulated Raman scattering (SRS) cross talk. In comparison to FWM and XPM, SPM only imposes minor degradations in the investigated setups. SRS mainly imposes a tilt in the spectrum, which is usually compensated by a flattening filter or an inverse tilt of the gain spectrum of the EDFA.

The individual degradations are combined to a single FOM. In a first step the Q factor due to ASE noise is determined from the OSNR:

$$Q_{\text{noise}} = \sqrt{\frac{f_{\text{opt,ref}}}{2f_{\text{el}}}}\text{OSNR} \approx \frac{\mu_1}{\sigma_{1,\text{ASE}}}, \tag{13}$$

where $f_{\text{opt,ref}}$ is the optical filter bandwidth (here $f_{\text{opt,ref}}=12.5$ GHz) and f_{el} is the (double-sided) electrical filter bandwidth (here $f_{\text{el}}=14$ GHz). Afterwards the Q factor is converted to logarithmic units and Q-factor penalties for the other effects (XPM, FWM, filter cross talk) are calculated and subtracted from Eq. (13):

$$Q_{\text{Penalty,dB}} = 20 \log Q_{\text{Penalty,linear}}. \tag{14}$$

For the nonlinear effects of XPM and FWM the Q-factor penalties are given by calculating the ratio of the Q factor including nonlinear degradation and the Q factor without the regarded nonlinear effect. Because it is assumed that XPM and FWM do not change the average signal power but only add noise to the mark level, the penalties are obtained from

$$Q_{\text{Penalty,linear}} = \frac{Q(\sigma^2_{\text{nonlinear effect}})}{Q(\sigma^2_{\text{nonlinear effect}} = 0)} = \frac{\sigma_{1,\text{ASE}}}{\sqrt{\sigma^2_{1,\text{ASE}} + (R2P_{\text{rec}})^2 \sigma^2_{\text{nonlinear effect}}}}. \quad (15)$$

In Eq. (15) the variance $\sigma^2_{\text{nonlinear effect}}$ of the detected mark symbols due to XPM and FWM [compare Eqs. (7) and (12)] is used. Furthermore, a variance of the detected marks due to noise $\sigma^2_{1,\text{ASE}}$ is introduced, which can be calculated easily from Eq. (13), if ASE noise on the space symbols is assumed to be small. The second summand in the denominator of Eq. (15) stems from fiber nonlinearity and accounts for the increase of the signal power variance due to nonlinearities (remember that variances add quadratically). The advantage of such a procedure is that the noise penalty is modeled for the individual wavelength (or WDM channel) from the source node to the destination node. This enables one to track the ASE noise correctly, which has been accumulated along the path in the individual channel. The penalties due to the other degradation effects are modeled either as fixed (worst-case) penalties for each link (offline routing) assuming a fully loaded system or based on the current network status (online routing). Nonlinear degradations caused by FWM or XPM tend to saturate for an increasing number of WDM channels (approximately more than 10 channels). If further channels are added, the worst-case penalty will remain the same. In our investigations we assume a minimal transmission quality requirement of bit error ratio (BER) $= 10^{-9}$ (prior to forward error correction) in the following equivalent to a Q factor of $Q_{\text{min}} = 15.56$ dB.

3.F. Different Routing Algorithms

In this work, three different routing algorithms have been investigated. The simplest one is based on a shortest-path algorithm combined with the constraint of wavelength continuity along the entire desired transparent path. The algorithm computes the k shortest (disjoint) paths (here $k = 3$) first, and afterwards it tries to find a continuous wavelength along the paths. If a regenerator pool is available along the calculated path, wavelength continuity is only required for the transparent subpaths. If the first path does not meet the wavelength continuity and maximal transparent distance constraints, the second and then the third path are tested. If all three candidate paths cannot be set up, the demand is blocked.

Furthermore, we investigated CBR algorithms based on worst-case physical transmission penalties (offline routing) or the current network status (online routing). Obviously the latter approach is computationally more challenging because the transmission quality has to be calculated on the fly when a connection request occurs. The computational time of the online routing approach is mainly limited by the calculation of the XPM degradation (compare Subsection 3.B) growing with the square of the number of spans and the square of the number of channels. In contrast to that the offline routing approach only needs to sum the worst-case contributions of the nonlinear effects, which can be precomputed, and to add them to the degradation due to ASE and filter cross talk. This is why only in the case of a rejection of a connection based on the worst-case penalties is the online routing started for this connection request to reduce the computational time. The more exact online routing can then determine whether the desired connection really has to be rejected or the current traffic situation will permit setting up the connection request.

A flow chart for the online routing algorithm is shown in Fig. 4. The algorithm starts with finding the k shortest paths (this time taking the worst-case Q-factor penalties as edge weights instead of the actual lengths) between the source and destination nodes, which can be precomputed. As in the shortest-path algorithm, thereafter the wavelength continuity along the transparent paths is checked. If no free (continuous) wavelength can be found, the connection is blocked. In the next step the Q factor at the destination node is calculated as outlined in Subsection 3.E taking into account the worst-case degradation for a fully loaded system, which also can be precomputed. Subsequently it is tested to determine whether the Q factor lies above the threshold. If this is the case, the connection is established. If not, the connection request is rejected in the offline routing scenario. If, however, the online routing algorithm is selected, another assessment of the signal quality at the destination node is performed at this time based on the current traffic situation. If this second check yields that the Q factor is higher than the threshold (e.g., due to a low number of used wave-

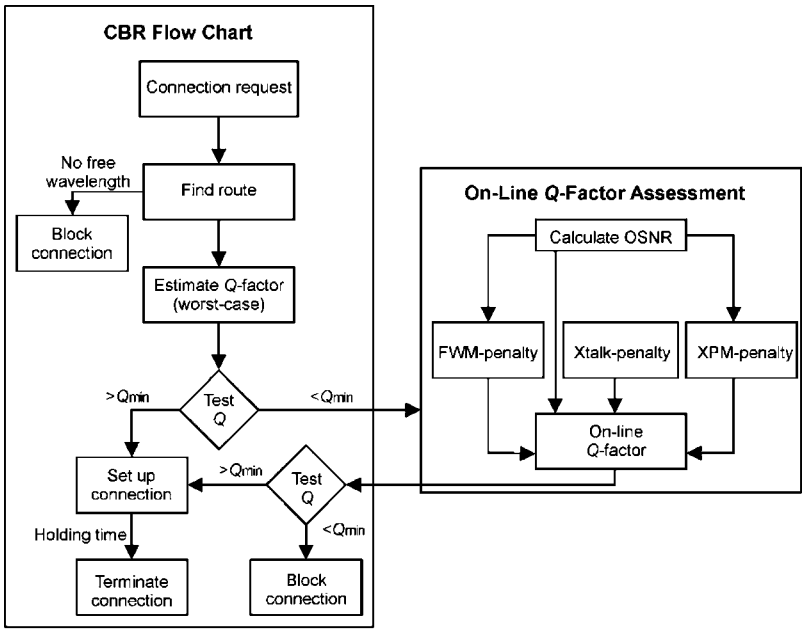

Fig. 4. Flow chart of the online CBR algorithm.

lengths and a resulting low nonlinear degradation), the connection can be set up. Otherwise it is ultimately rejected. If the connection is established, it is torn down after a negative exponential holding time.

Concerning the computational time, the offline routing algorithm is very efficient because it is mainly based on lookup tables (for the shortest paths and the penalties). The online routing algorithm is much more challenging, involving calculations with complex numbers and Fourier transforms. However, the routing of a single demand and the calculation of the online penalties can still be performed well below 1 s on a current desktop computer. Typically, only a fraction of the demands will require online assessment of the signal quality because offline routing will already permit setting up the desired connection.

For the arrivals of the connection requests, a Poisson process [15] with an average interarrival time of 1 time unit and for the holding times negative exponential distributions with a mean of 1 time unit are assumed. Thus, in the initial state the offered load (i.e., the product of mean holding time and arrival rate) is 1. Furthermore, the interarrival times are divided by a linear demand scaling factor S to assess the blocking probability in the future when the total network traffic has increased (as suggested by [16]). In the initial state ($S=1$) this corresponds to a traffic load of 0.063 Erlang per node, which is increased to 10.08 Erlang in the simulations ($S_{\max}=160$). The demand scaling factor can be used to investigate the performance of the network in the future when the traffic has increased by a factor of S. In our investigations unprotected services have been assumed. In all cases the granularity of the demands has been chosen to be 10 Gbits/s.

4. Regenerator Placement

Up to this point fully transparent optical networks have been assumed. However, in reality it is difficult to deploy fully transparent networks because transmission impairments restrict the maximum reach of a transparent light path. On the contrary OEO regeneration imposes high costs. That is why as few regenerators as possible are deployed. An OXC including an OEO regenerator pool is depicted in Fig. 3 [17]. We assumed that regeneration is only available for a limited number of channels. The regenerator bank is colorless, meaning that any arriving wavelength may be passed to the regenerator. Furthermore, the regenerator bank may be used as a tunable wavelength converter.

The selection of the regeneration sites is based on the evaluated physical impairments. For a given connection between two nodes that is longer than the optical

reach, there are several regeneration options [18]. However, due to restrictions in capital expenditure (CAPEX) and operational costs (OPEX) the total number of regenerator sites is kept as low as possible and an attempt is made to concentrate regenerators at a limited number of nodes only.

A heuristic approach has been employed inspired by [19] to place the regenerators (Fig. 5). A new graph is created with the location of the nodes defined by the investigated reference network. Then the algorithm tries to set up a complete graph with edges between any combinations of the nodes under the constraint that the minimal Q factor ($Q = 15.56$ dB) is exceeded. If the constraint is broken, the regarded connection can only be established if a regenerator is placed along the link. The first regenerator is placed at the node that will enable one to establish the maximum of previously blocked connections if a regenerator were available there. Afterwards the procedure is repeated and the second regenerator is placed at that location, which will enable one to set up the maximum of previously blocked connections and so forth. In most cases there remains some flexibility to place the regenerator at different positions along the route. In this case an attempt is made to minimize the total number of regenerator sites and to concentrate regeneration at a limited number of nodes only (maximizing the number of feasible connections) to reduce costs related to installation and maintenance. In our investigations we did not optimize the number of regenerator ports, meaning that all regenerator sites allow regeneration of all 80 wavelengths. Furthermore, no specific traffic matrix has been considered for placing the regenerator pools. In a dynamic network there is no knowledge of the traffic matrix *a priori* and the demands arise dynamically. The objective is to achieve full connectivity, meaning that it should be possible to set up a connection between any combinations of two nodes.

In Fig. 6 the nodes equipped with repeaters for a SSMF-based network are depicted and marked by red squares. A total number of eight regeneration sites are placed, which is in line with other publications [20], suggesting that it is enough to place regenerators at 20% of the nodes to achieve a performance comparable to an opaque network. With these eight regenerator pools it is possible to achieve full connectivity in the investigated SSMF-based network (for the shortest paths between any two nodes). Looking back at Fig. 2, where a huge number of paths fall below the threshold, at this time all shortest paths between any two nodes will lie above the threshold. If, however, the shortest path is unavailable and a detour has to be taken, blocking may still occur. This is where the CBR algorithm comes into play and has to find an alternative route, which fulfills the signal quality requirements. The effect of regeneration regarding the blocking probability is twofold. First, certain connections can only be established with OEO regeneration due to restrictions in the transparent reach. Second, regenerators also enable wavelength conversion. In this way the wavelength continuity constraint is somehow relaxed. However, we could not observe a significant reduction of the blocking probability due to the relaxed wavelength continuity requirement. The reason is that it is possible to take a detour, if a wavelength is blocked along the shortest path (remember, the three shortest paths are considered).

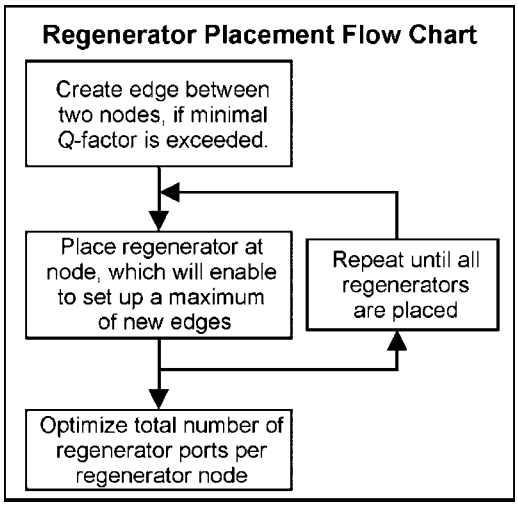

Fig. 5. Flow chart of the regenerator placement algorithm.

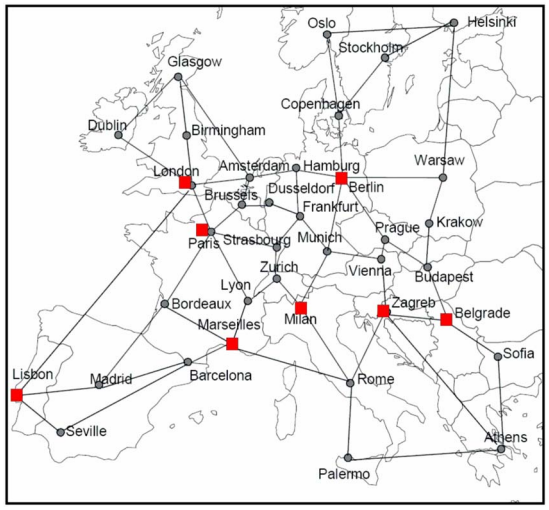

Fig. 6. COST266 reference network with selective regeneration at certain nodes (red squares), SSMF transmission fiber.

Only in the case of very high demand scaling factors, no continuous wavelength may be found on all three shortest paths, and blocking will occur.

In the case of NZDSF transmission fibers, different regenerator positions have been calculated. Our heuristic suggests placing 25 regenerators to achieve full connectivity. Due to cost considerations and allowing a fair comparison to the above SSMF-based network, however, we only deployed eight regenerators in the NZDSF-based network, resulting in limited connectivity (i.e., it is not possible to set up a connection between any combinations of nodes leading to a considerable base blocking probability as shown below).

5. Results

We analyzed two networks with either SSMF or NZDSF including regenerator pools at the locations indicated in Figs. 6 and 7. Furthermore, three different routing algorithms (as described in Subsection 3.F) have been assessed based on the link lengths only (termed "shortest path" in the following), worst-case physical constraints (offline), and the current network load (online). In all cases, wavelength continuity along the transparent paths has been assumed as a requirement.

To assess the quality of the routing algorithms we also performed simulations for an ideal (opaque) network without any physical impairment (Fig. 8). We have found that in the opaque scenario the increasing traffic does not lead to a higher blocking

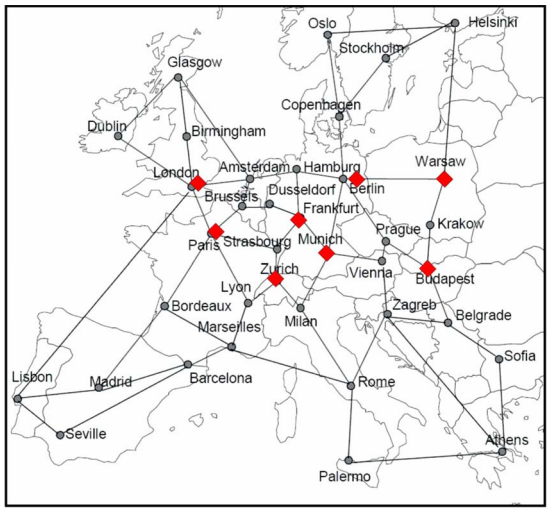

Fig. 7. COST266 reference network with selective regeneration at certain nodes (red diamonds), NZDSF transmission fiber.

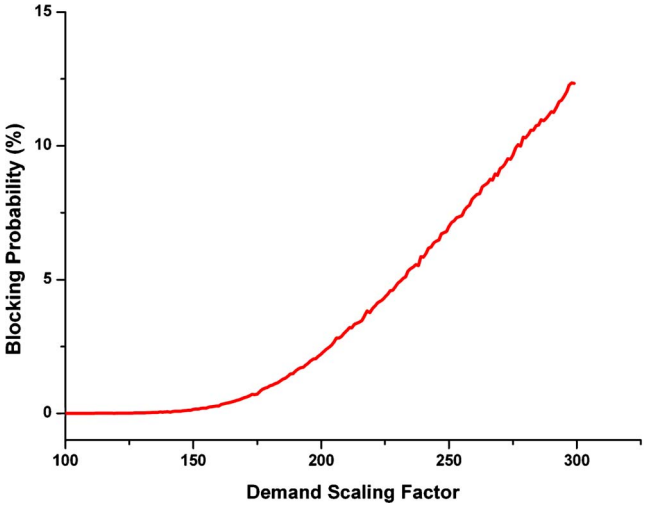

Fig. 8. Impact of growing traffic on the blocking probability in an ideal network (without any physical impairments). The mean value of 120 random realizations is depicted. The 95% confidence intervals are not depicted because they are extremely small.

probability up to a demand scaling factor S of 150. For even higher demand scaling factors the limited availability of network resources leads to an exponential increase of the blocking probability.

In all further simulations the translucent network with selective regeneration at eight locations is used. Without selective regeneration, a blocking probability of more than 50% for SSMF-based networks and 70% for NZDSF-based networks is observed because a large number of demands cannot be routed due to limited transparent reach. This makes it clear that intelligent regenerator placement is the base for good performance of a CBR algorithm. In a first set of simulations the shortest-path algorithm has been applied. With this algorithm a blocking probability of approximately 33% in the investigated parameter range ($1<S<160$) has been observed for SSMF-based networks (75% for NZDSF), which is clearly unacceptable for most types of applications. In the regarded range of the demand scaling factor S, the blocking probability remained more or less independent of S. Looking back at Fig. 2 this behavior can be understood easily. As maximal bridgeable transmission distance in the worst case only 1280 km is feasible for SSMF (725 km for NZDSF). All other connections with higher path lengths have to be rejected or routed via a regenerator leading to a high blocking probability due to an insufficient number of regenerators.

In the following paragraph the results from the online and offline CBR algorithms are discussed. In Figs. 9 and 10 the blocking probability is shown as a function of the demand scaling factor. Also the confidence intervals (at 95% confidence level) are

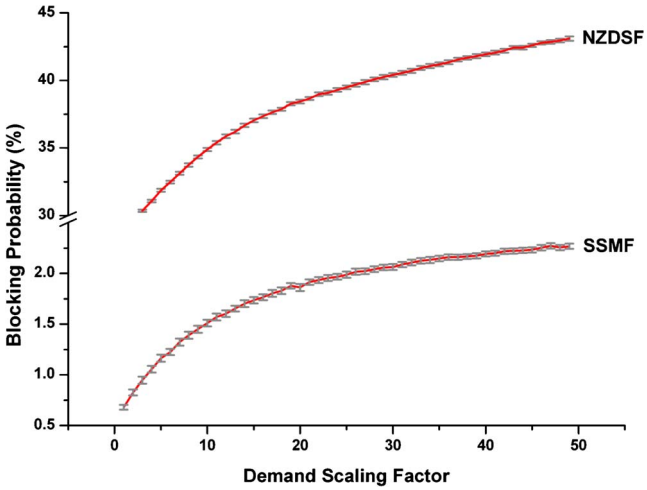

Fig. 9. Comparison of the blocking probability for the investigated routing algorithms (offline routing). Also depicted are the 95% confidence intervals.

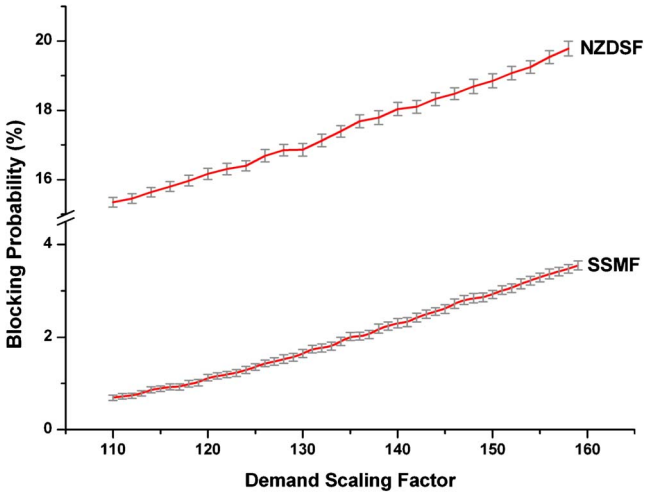

Fig. 10. Comparison of the blocking probability for the investigated routing algorithms (online routing). Also depicted are the 95% confidence intervals.

depicted. It can be observed that both—online (Fig. 10) and offline (Fig. 9) CBR—show much lower blocking probabilities than the shortest-path algorithm. Because of the lower local dispersion of NZDSF compared to SSMF, the fiber nonlinearities are more severe, resulting in shorter reach and a higher blocking probability for this type of fiber. The nonlinear FWM effect in particular has a significant impact if NZDSF is employed due to a high-phase-matching between the different WDM channels. If SSMF are used, FWM does not impose considerable signal degradation. Furthermore, the lower local dispersion of NZDSF leads to a reduced walk-off between the WDM channels increasing the XPM effect. Only the degradation due to ASE is somewhat reduced because of the shorter DCF lengths needed in NZDSF-based networks and the corresponding lower attenuation of the DCF modules. Taking these effects together it can be explained why the blocking probability of approximately 2% for SSMF is increased to 42% for NZDSF (if a demand scaling factor of 50 and offline routing are assumed).

It is expected that the total traffic will steadily increase with growth rates of 30% to 100% per year in the future. Our investigations also show that for much higher traffic than originally defined ($S=1$) in [5] the blocking probability will remain in a range that is acceptable for dynamically switched translucent networks (below 3% as suggested in [16]). The results for the online routing CBR algorithm have been obtained up to a demand scaling factor of 160 (equivalent to a traffic volume of 160 times the original value). Compared to the offline routing algorithm, the online algorithm yields acceptable blocking probabilities (below 3%) up to a much higher demand scaling factor of up to $S=160$ instead of $S=50$ in the offline case. This can be explained by considering the current traffic situation in online routing. Especially for a low number of active channels the online assessment of the Q factor will exhibit a significantly lower degradation due to the nonlinear effects compared to the worst case (offline) in turn leading to a lower blocking probability. Comparing the different reasons for wavelength blocking (physical layer degradation, network resources), it turns out that physical layer blocking is dominant for demand scaling factors up to $S \approx 200$. Afterwards the lack of network resources becomes dominant.

6. Conclusion

Different CBR algorithms in combination with intelligent, physical-impairment-based, regenerator placement have been investigated. Intelligent regenerator placement yields full connectivity in the examined (SSMF) topology with only regenerator pools placed at eight nodes (out of a total of 37 nodes). The proposed new CBR algorithms are suitable for on-the-fly network operation because a majority of the computational work can be precomputed, and only in the case of a rejection of a connection the signal quality has to be computed on-line based on the current network loading conditions. It is shown that the proposed CBR algorithm—taking into account the actual network condition—can significantly decrease the blocking probability. Also a

simpler approach based on a worst-case approximation of the signal impairments yields a significantly lower blocking probability compared to shortest-path routing. Our novel approach enables consideration of a heterogeneous infrastructure with different fiber types and a varying dispersion map. The exact assessment of the signal quality based on the current traffic situation using fast analytical methods permits up to five times more traffic (for a blocking probability of 3%) in a network compared to routing with worst-case estimations. Hence a precise estimation of the signal quality degradation may have a strong impact on the provider's profits.

References

1. C. T. Politi, H. Haunstein, D. A. Schupke, A. Stavdas, M. Gunkel, J. Martensson, A. Lord, and J. Martensson, "Integrated design and operation of a transparent optical network: a systematic approach to include physical layer awareness and cost function," IEEE Commun. Mag. **45**(2), 40–47 (2007).
2. I. Tomkos, S. Sygletos, A. Tzanakaki, and G. Markidis, "Impairment constraint based routing in mesh optical networks," in *Proceedings of the Optical Fiber Communication Conference* (Optical Society of America, 2007), paper OWR 1.
3. C. T. Politi, V. Anagnostopoulos, C. Matrakidis, and A. Stavdas, "Physical layer impairment aware routing algorithms based on analytically calculated *Q*-factor," in *Proceedings of the Optical Fiber Communication Conference* (Optical Society of America, 2006), paper OFG 1.
4. G. Markidis, S. Sygletos, A. Tzanakaki, and I. Tomkos, "Impairment constraint routing in 2R-based long haul optical networks," in *Proceedings of the European Conference on Optical Communication* (2006).
5. COST266: Pan-European reference networks, http://sndlib.zib.de.
6. A. Dwivedi and R. E. Wagner, "Traffic model for USA long-distance optical network," in *Proceedings of the Optical Fiber Communication Conference* (Optical Society of America, 2000), paper TuK1-1.
7. S. Pachnicke, J. Reichert, S. Spälter, and E. Voges, "Fast analytical assessment of the signal quality in transparent optical networks," J. Lightwave Technol. **24**, 815–824 (2006).
8. E. Desurvire, *Erbium-Doped Fiber Amplifiers Principles and Applications* (Wiley, 1994).
9. A. V. T. Cartaxo, "Cross-phase modulation in intensity modulation-direct detection WDM systems with multiple optical amplifiers and dispersion compensators," J. Lightwave Technol. **7**, 178–190 (1999).
10. S. Pachnicke, T. Gravemann, M. Windmann, and E. Voges, "Physically constrained routing in 10-Gb/s DWDM networks including fiber nonlinearities and polarization effects," J. Lightwave Technol. **24**, 3418–3426 (2006).
11. J. Proakis, *Digital Communications* (McGraw-Hill, 1995).
12. G. P. Agrawal, *Nonlinear Fiber Optics*, 3rd ed. (Academic, 2001).
13. W. Zeiler, F. Di Pasquale, P. Bayvel, and J. E. Midwinter, "Modeling of four-wave mixing and gain peaking in amplified WDM optical communication systems and networks," J. Lightwave Technol. **14**, 1933–1996 (1996).
14. M. Vasilyev, I. Tomkos, M. Mehendale, J.-K. Rhee, A. Kobyakov, M. Ajgaonkar, S. Tsuda, and M. Sharma, "Transparent ultra-long-haul DWDM Networks with broadcast-and-select OADM/OXC architecture," J. Lightwave Technol. **21**, 2661–2672 (2003).
15. L. Kleinrock, *Queueing Systems* (Wiley, 1975).
16. D. A. Schupke, M. Jäger, and R. Hülsermann, "Comparison of resilience mechanisms for dynamic services in intelligent optical networks," in *Proceedings of the Fourth International Workshop on Design of Reliable Communication Networks* (IEEE, 2003).
17. Y. Ouyang, Q. Zeng, and W. Wei, "Dynamic lightpath provisioning with signal quality guarantees in survivable translucent optical networks," Opt. Express **13**, 10451–10468 (2005).
18. J. M. Simmons, "Network design in realistic all-optical backbone networks," IEEE Commun. Mag. **44**(11), 88–94 (2006).
19. S. Chen and S. Raghavan, "The regenerator location problem," Working paper, Smith School of Business, University of Maryland (2006).
20. B. Ramamurthy, S. Yaragorla, and X. Yang, "Translucent optical WDM networks for the next-generation backbone networks," in *Proceedings of IEEE GlobeCom* (IEEE, 2001).